PCH PhysicoChemical Hydrodynamics Vol. 5, No. 1, pp. 53–66, 1984.
Printed in Great Britain

0191-9059/84 $3.00 + 0.00
Pergamon Press Ltd.

4084

HYDRODYNAMICS AND HEAT TRANSFER IN ENCLOSURES CONTAINING A FIRE SOURCE

N. C. MARKATOS*

Concentration Heat and Momentum Limited, 40 High Street, Wimbledon, London SW19 5AU, England

and

G. COX

Fire Research Station, Borehamwood, Hertfordshire, England

(*Received* 15 *June* 1983)

Abstract—The paper is concerned with the prediction of steady-state or transient, three-dimensional flow and heat transfer in enclosures of arbitrary complexity containing a fire source. The prediction method is based on a finite-domain solution of the three-dimensional fluid dynamic and heat/mass transfer field equations, with full effects of compressibility included and with modelling of the turbulence-buoyancy interactions.

Results are presented for two compartment geometries as demonstrations of the potential of the method and also as preliminary validation comparisons with steady-state experiments.

It is concluded that more work is required to validate the model against more experimental results, and that the successful application of a fully three-dimensional steady-state or transient "field-model" to fire problems with multiple parameters does not require prohibitively great computer power.

1. INTRODUCTION

The modelling of fire spread within a building presents a formidable challenge for mathematicians, physicists and engineers. Not only are the underlying physical processes difficult to model (turbulent buoyant convection, radiative transfer, combustion), but imponderables such as the location of the fire within the room of origin, the external wind conditions, and the configuration of each door and window will affect the outcome.

There are two distinct approaches to the problem, known as stochastic and deterministic modelling. Stochastic or 'random process' modelling does not attempt to examine the governing physical or chemical processes controlling fire but assembles a series of empirically determined probabilities of a specific occurrence (e.g. flame spread from item to item as a function of spacing) to form an overall model of fire behaviour. Deterministic models on the other hand predict fire behaviour for a prescribed situation, effectively the mathematical counterpart of a laboratory experiment or test.

There are different types of model within these broad classifications, perhaps the most important difference being between the so-called zone and field deterministic models. Both solve a series of equations describing the physics of the problem, the difference between them being in the rigour and generality of these equations. Zone models, the most comprehensive of which has been developed by Emmons and coworkers [1], rely heavily on experimentally determined empirical expressions whilst field models, for the most part, do not. Field models

* Present address: School of Mathematics, Statistics & Computing, Thames Polytechnic, London SE18.

solve the underlying equations of motion and conservation for the system. The number of calculations made with this approach is very large resulting in relatively longer computing times but the model is far more generally valid than the zone model.

The modelling of smoke movement within buildings by the latter approach represents an important first step towards the longer-term objective of predicting the spread of fire, as well as being an important end in itself; more than 50% of the fire deaths in the U.K. can be attributed to smoke. Furthermore, the model would enable various geometrical configurations and conditions to be assessed without the need for expensive and necessarily incomplete physical model tests.

Such a mathematical model, restricted to two space dimensions, has already been used to model smoke movement in enclosures [2]. Extensive numerical computations have been performed for several configurations of interest, and the results showed fair agreement with what limited experimental data were available. Most experiment data, however, have strong three-dimensional features and cannot be used satisfactorily for two-dimensional model development and validation. For the above reasons it is considered imperative to develop efficient three-dimensional models both for end-use and for validation against existing three-dimensional experimental data. This paper describes the development of such a three-dimensional mathematical model and demonstrates its practical capability together with some comparisons with experiment.

2. THEORETICAL FOUNDATION OF THE MODEL

2.1. *The physical problem*

The physical problem concerns the movement of combustion products in three-dimensional enclosures of arbitrary geometrical complexity. In this problem the flow is dominated by buoyancy and the turbulence serves to promote the rate of diffusion of heat (or smoke concentration), mass and momentum. Neither radiation nor combustion are included at this stage, the fire source being represented in the model by a volumetric mass or heat source. Non-uniform buoyancy forces are allowed to affect both the mean flow and the fluctuating motions.

2.2. *The governing differential equations*

The independent variables of the problem are the three components (x, y, z) of a Cartesian coordinate system, and time (t). The main dependent variables characterising the flow are the three velocity components (u, v, w), the pressure p, the smoke concentration f or enthalpy h, the kinetic energy or turbulence k, and the energy dissipation rate ε.

All these dependent variables, with the exception of pressure, appear as the subjects of differential equations of the general form

$$\frac{\partial}{\partial t}(\rho\phi)+\operatorname{div}(\rho\mathbf{u}\phi+\mathbf{J}_{\phi}) = S_{\phi} \tag{1}$$

where ϕ stands for a generic fluid property and ρ, $\mathbf{u}$, $\mathbf{J}_\phi$, S_ϕ are density, velocity vector, diffusive-flux vector and source rate per unit volume, respectively.

The diffusive-flux $\mathbf{J}_\phi$ is given by

$$\mathbf{J}_\phi = -\Gamma_\phi \operatorname{grad} \phi \tag{2}$$

where Γ_ϕ denotes the 'effective exchange coefficient of ϕ' determined from the set of turbulence parameters (k, ε), which are themselves dependent variables of differential equations of the form of equation (1) [3–5]. The values of ϕ, Γ_ϕ and S_ϕ are listed in Table 1, where

$$\mu_{eff} = \mu_t + \mu_l, \mu_t = C_D \rho k^2/\varepsilon \tag{3}$$

$$G_K = \mu_t\left\{2\left[\left(\frac{\partial u}{\partial x}\right)^2 + \left(\frac{\partial v}{\partial y}\right)^2 + \left(\frac{\partial w}{\partial z}\right)^2\right] + \left[\left(\frac{\partial u}{\partial z}\right)^2 + \left(\frac{\partial w}{\partial x}\right)^2\right] + \left[\left(\frac{\partial w}{\partial y}\right)^2 + \left(\frac{\partial v}{\partial z}\right)^2\right] + \left[\left(\frac{\partial u}{\partial y}\right)^2 + \left(\frac{\partial v}{\partial x}\right)^2\right]\right\} \tag{4}$$

$$G_B = \mu_t g \frac{1}{\rho}\frac{\partial \rho}{\partial y} \text{(see [2])}. \tag{5}$$

The turbulence model contains five empirical constants which are assigned the following values [2]:

$$C_1 = 1.44, C_2 = 1.92, C_D = 0.09, \sigma_k = 1.0, \sigma_\varepsilon = 1.3. \tag{6}$$

The term $\dot{q}'''$ in Table 1 represents a volumetric heat source/sink. The dilation terms have been ignored. Work with the two-dimensional model [2] proved that they are completely insignificant in the flows under consideration.

The pressure variable is associated with the continuity equation

$$\frac{\partial \rho}{\partial t} + \operatorname{div}(\rho \mathbf{u}) = 0 \tag{7}$$

in anticipation of the so-called pressure correction equation [6] which is deduced from the finite-difference form of equation (7).

Table 1. Values of ϕ, Γ_ϕ and S_ϕ

ϕ	Γ_ϕ	S_ϕ
1	0	0 (continuity)
u	μ_{eff}	$-\frac{\partial p}{\partial x} + \frac{\partial}{\partial x}\left(\mu_{eff}\frac{\partial u}{\partial x}\right) + \frac{\partial}{\partial y}\left(\mu_{eff}\frac{\partial v}{\partial x}\right) + \frac{\partial}{\partial z}\left(\mu_{eff}\frac{\partial w}{\partial x}\right)$
v	μ_{eff}	$-\frac{\partial p}{\partial y} - g(\rho - \rho_{ref}) + \frac{\partial}{\partial x}\left(\mu_{eff}\frac{\partial u}{\partial y}\right) + \frac{\partial}{\partial y}\left(\mu_{eff}\frac{\partial v}{\partial y}\right) + \frac{\partial}{\partial z}\left(\mu_{eff}\frac{\partial w}{\partial y}\right)$
w	μ_{eff}	$-\frac{\partial p}{\partial z} + \frac{\partial}{\partial x}\left(\mu_{eff}\frac{\partial u}{\partial z}\right) + \frac{\partial}{\partial y}\left(\mu_{eff}\frac{\partial v}{\partial z}\right) + \frac{\partial}{\partial z}\left(\mu_{eff}\frac{\partial w}{\partial z}\right)$
h	$\left(\frac{\mu_l}{\sigma_l} + \frac{\mu_t}{\sigma_t}\right)$	$\dot{q}'''$
k	$\frac{\mu_{eff}}{\sigma_k}$	$G_k - \rho\varepsilon + G_B$
ε	$\frac{\mu_{eff}}{\sigma_\varepsilon}$	$\frac{\varepsilon}{k}((G_k + G_B)C_1 - C_2\rho\varepsilon)$

3. METHOD OF SOLUTION

3.1. *Formulation of equations*

The space and time dimensions are discretized into finite intervals and the variables are correspondingly computed at only a finite number of locations in four-dimensional space, i.e. at the so-called 'grid-points'. These variables are connected with each other by algebraic equations, derived from their differential counterparts by integration over the control volumes defined by the above-mentioned intervals. Further details may be found in [6, 7].

3.2. *The solution procedure*

The procedure adopted for the solution of the equations is the SIMPLEST algorithm [8]. The difference of this procedure from the well-established SIMPLE [6] is that the finite-domain coefficients of the momentum equations contain only diffusion contributions, the convection terms being added to the linearized source term of the equations. This practice was found to eliminate the need for severe underrelaxation of the pressure correction, particularly for very fine grids, thus accelerating convergence.

For the transient procedure a fully-implicit formulation was adopted. This means that where any latitude exists at all in the finite-domain equations late-time values are taken. This formulation has the advantage over explicit or semi-implicit ones that the time step need be no smaller than that dictated by accuracy requirements.

Further details on the solution procedure may be found in [2, 6, 8].

3.3. *Boundary conditions*

To complete the mathematical analysis, it is necessary to provide boundary conditions. For the present problem, there are two types of boundary: solid or free. On a *solid boundary*, the non-slip condition on the velocity components is employed. For the energy equation, a fixed temperature of 293 K is assumed at the outside surface of all walls enclosing the fire compartment, except for the floor which is assumed adiabatic. The fluxes of momentum and heat to the walls obey the wall-function relations of Launder and Spalding [9], and the heat losses through the fire-compartment walls are calculated from given wall conductivity and thickness and the computed temperature gradients.

For the kinetic energy of turbulence, a zero diffusive flux at the wall is used. For the dissipation rate, the empirical evidence that a typical length scale of turbulence varies linearly with the distance from the wall, is used to calculate ε itself at the near-wall point.

It is realised that with temperature stratification the equivalent of the 'law of the wall' is the Monin–Obukov log-linear profile [10]. However, at present the conventional log law is employed, as generalized in [9].

The above considerations lead directly to the computation of wall shear stress $(\tau/\rho)_w$, and of the heat flux $\dot{q}''_w$

$$(\tau/\rho)_w = \frac{U_P C_D^{1/4} k_P^{1/2} \kappa}{\ln\left[E\delta \dfrac{(C_D^{1/4} k_P^{1/2} \rho)}{\mu_l}\right]} \tag{8}$$

$$\dot{q}''_w = (T_P - T_w) C_P \rho C_D^{1/4} k_P^{1/2} / \sigma_t \left[\frac{1}{\kappa} \ln \frac{(E\delta C_D^{1/4} k_P^{1/2} \rho)}{\mu_l} + P_j\right] \tag{9}$$

where subscripts w, P refer to conditions at the wall and at the near-wall point at a distance δ, respectively. E, κ are constants with values 9.0 and 0.42 respectively; μ_l is the fluid viscosity;

and P_j is a function of the laminar and turbulent Prandtl numbers, obtained by Jayatillaka [11] from the study of wall heat transfer data. The value of this function is calculated here to be -2.95.

The Stanton number is calculated from equations (8) and (9), and is given by:

$$St = \frac{S}{\sigma_t} \Big/ (1 + P_j S^{1/2}) \tag{10}$$

where S is the friction factor ($S = \tau/\rho U_P^2$).

On the *free-boundary* a fixed-pressure boundary condition is imposed; the mass inflows and outflows being an outcome of the solution procedure.

3.4. *Initial conditions*

For the steady-state, computations start with the solutions of a previous run as initial condition. When making the first calculation initial velocity fields are deduced from a simple extension to three-dimensions of the stream function guess described in [2]. The temperature is set initially by assuming a vertical relationship with height, ranging from 800 K to ambient.

3.5. *Physical properties*

The fluid viscosity is taken as 1.82×10^{-5} kg/ms and the Prandtl number as 0.7. A constant specific heat of $C_P = 1100$ J/kgK is used.

The local density is linearly dependent upon the reciprocal of the specific enthalpy:

$$\rho = \frac{pC_P}{Rh} \tag{11}$$

where $R = 287$ J/kg K.

4. RESULTS AND VALIDATION

Two distinct compartment geometries have been examined for demonstration and validation purposes. The first is an enclosed 'shopping mall' of 'L shaped' geometry, see Fig. 1. This compartment has been used here largely for demonstration purposes since, although many data have been obtained in it by Heselden and his coworkers [12], the problems of measuring hot gas velocity were still unresolved, at the time of the work, and so this aspect of any validation exercise would remain uncertain.

The second compartment is the roughly cubical room used by Steckler *et al.* [13] (Fig. 2) for their more recent, thoroughly instrumented fire experiments. This study gave more data with which the predictions of the model could be compared. Details of the computations and comparisons follow.

4.1. *Shopping mall*

The shop 4 × 8 × 3 m high with an opening onto one side of a mall 16 m long, 6 m wide and 3 m high contains a heat source to represent the fire (Fig. 1). The coordinate system has its origin at the left-hand corner of the shop's floor, with the z-axis directed along the mall. The implication of this choice on the solution procedure is that it involves what are called 'repeated z-direction sweeps' through the integration domain. The whole set of finite-domain cells is regarded as consisting of one-cell-thick 'slabs', extending in the x and y directions, and

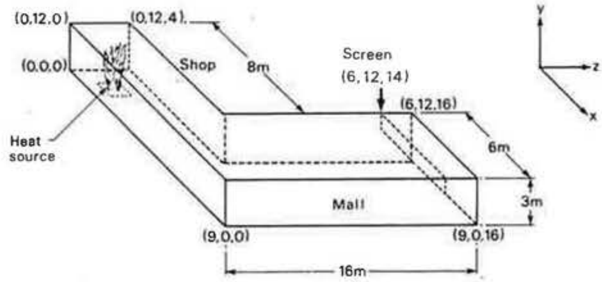

Fig. 1. Schematic diagram of shop and mall—(IX, IY, IZ) are co-ordinate grid nodes defining solution domain.

piled one next to the other in the z-direction. A single sweep therefore starts with attention being paid to the first z-slab of cells. The finite-domain equations are solved for all the cells in this slab, the values of ϕ's at the next slab being regarded as known. Attention then passes to the second slab, and so on, until the adjustment sweep has been completed. At the end of a sweep, of course, the final solution has not yet been achieved; so the process must be repeated until a reasonable degree of convergence is achieved. The structure of the computer program used allows for such 'sweeps' only in the z-direction, and it was decided to perform them in the direction of the open end of the mall. A solid screen, 1 m deep, is suspended from the ceiling of the mall, 2 m from its open end. This is to define a smoke reservoir from which extraction vents may eventually remove smoke. A volumetric heat source simulates the fire by releasing heat non-uniformly with height as suggested by the recent experimental measurements of Cox and Chitty [14]. The walls and ceiling are assumed to have a thermal conductivity of 1 W/mK, roughly representative of building brick or concrete together with a thickness of 0.1024 m. The floor and screen are assumed adiabatic.

Both steady and transient computations were performed for either a fixed heat-release rate of 3.2 MW or for a linearly growing fire reaching this same output at 3 min from 'ignition'. The source is distributed over a floor area of 1.6 m^2, in both cases, with its back edge located at a distance of 1.6 m from the rear wall (Fig. 1). For the transient problem not only did the local heat release vary with height but also the total height increased with time according to the flame length expression in [14].

Because of the exploratory nature of these computations only one grid, consisting of 1728 control cells ($9 \times 12 \times 16$), has been used. Grid-refinement studies are presented for the second validation case given below. The blocked region in the flow domain (and any other possible obstacle) is treated by use of 'cell porosities' [15]. In this approach, each cell in the domain is characterized by a set of fractions, in the range of 0 to 1. These fractions determine the proportion of the cell volume available for the fluid, and the proportion of each cell-face area available for flow, by convection or diffusion, from the cell to its neighbour in a given direction.

For the flow domain of Fig. 1, only porosities of either 0 or 1 are used; but any complicated geometry may be represented equally well by use of partial porosities.

Many results were obtained during the present study but space considerations dictate that only a fraction of these can be presented. Representative predictions with and without the screen in place are shown for the steady state in Figs 3–9. Figures 3 and 4 show the vertical and horizontal distributions, respectively, of the horizontal velocity components and of the temperature rise above ambient. These results are for an adiabatic thermal boundary condition at all walls. Figure 5 corresponds to the case with finite heat conductances through the shop walls, as described above; it represents the Stanton number distribution at the shop ceiling.

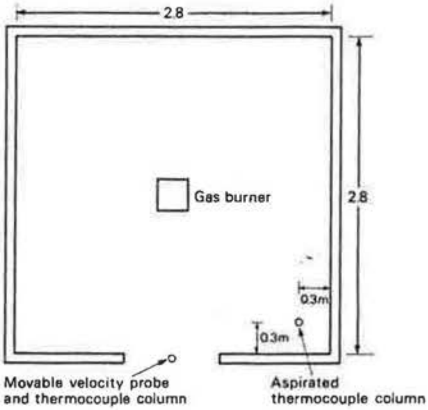

Fig. 2. Schematic plan view of Steckler's room with instrumentation.

The remaining figures are devoted to perspective plots of temperature and velocity vectors.

The main variables presented are the horizontal components of velocity (u, along the x-direction and w, along the z-direction), and the temperature rise above the ambient. Figure 3 presents the vertical distribution of these variables at two selected locations, namely at the shop entrance ($x = 8.75$ m, $z = 1.5$ m) and midway down the mall ($x = 11.75$ m, $z = 6.5$ m). Figure 4 shows the horizontal distribution of the same variables at near-floor ($y = 0.25$ m) and ceiling ($y = 3.0$ m) levels. The near-floor temperatures are not shown since they are always ambient.

Inspection of the above figures reveals the expected trends of high-temperature gases near the ceiling moving at around 2 m/s, with fresh air entering the system at ground level at around 1 m/s. There is clearly a strong horizontal velocity gradient across the mall due to the right-angled bend through which the gases turn.

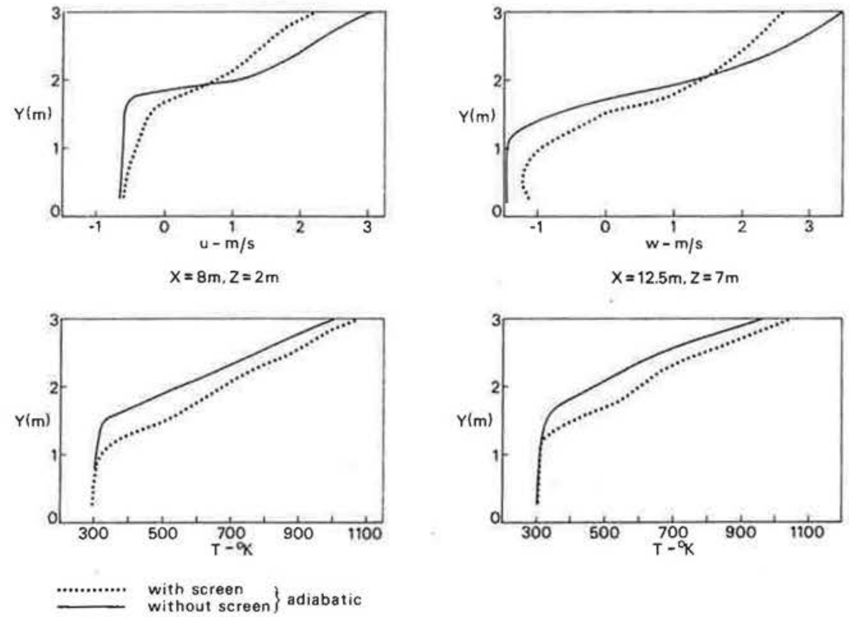

Fig. 3. Vertical scans of temperature and horizontal component of velocity.

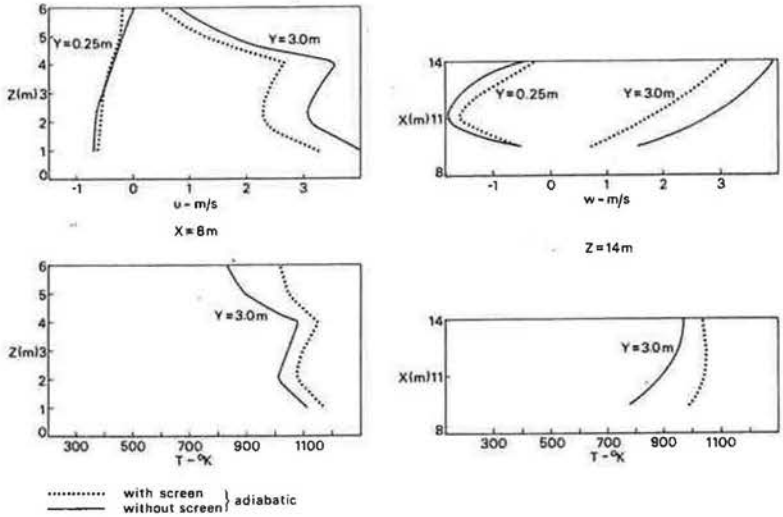

Fig. 4. Horizontal scans of temperature and horizontal component of velocity.

The results also show that the screen has the expected effects of increasing the hot gas temperature and reducing its velocity in the predominant flow direction.

High levels of turbulence viscosity (around 2000 μ_l) are also predicted here as in the two-dimensional work [2].

Results have also been obtained for finite heat conductances through the shop walls, but still with adiabatic conditions in the mall. A plot of Stanton number, calculated according to equation (10), at the shop ceiling ($y = 3.0$ m) is shown in Fig. 5, for the case with the screen in place.

It is worth noting that the maximum heat losses occur in the $x = 0$, $z = 0$ top corner, reflecting the experimentally observed tendency of the source plume to be drawn towards these walls. Figure 6 presents, in perspective view, surfaces of equal temperature ($T = 673$ K), over all x, y and z planes, for both cases (note that these plots are mirror images of Fig. 1, with different degrees of rotation, for clarity of viewing). The significant effect of the screen is immediately obvious. The top view of the same surfaces is also presented in the same figure.

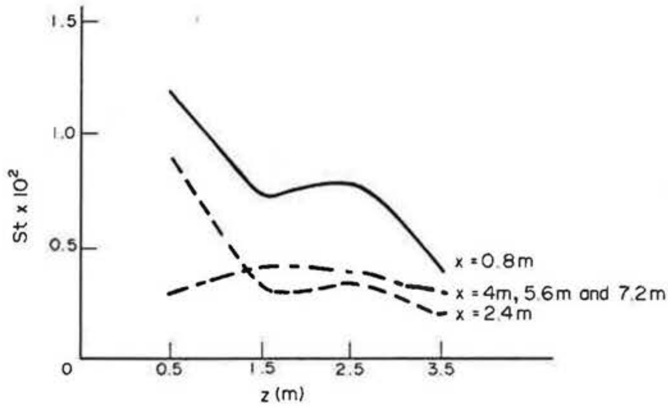

Fig. 5. Stanton number distribution at the shop ceiling.

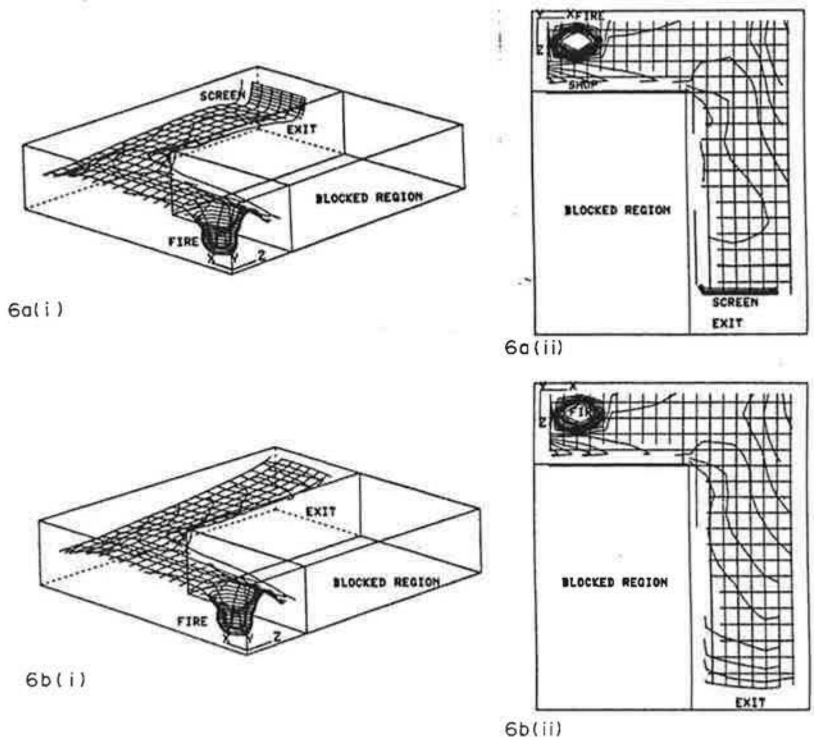

Fig. 6. Surfaces of equal temperature (T = 673 K) over all x, y and z-planes. (a) With screen in place. (b) Without screen.

Figure 7 presents velocity vectors as viewed from the side of the mall, at an x-location corresponding to 80% of the domain width.

For both cases, cold air is entering the mall over about 80% of the exit, and hot air leaves the mall at the top, at high speeds. For the case with the screen in place, it is clear that the gases turn because of the presence of the vertical screen; and also the effect of the screen in reducing the velocity in the predominant flow direction. Figure 8 presents velocity vectors, for the case without the screen, as viewed from the front of the system, at a z-location corresponding to 10% of the total length. The effect of the source on the velocity field is very pronounced and high velocities of around 5 m/s are observed in its vicinity.

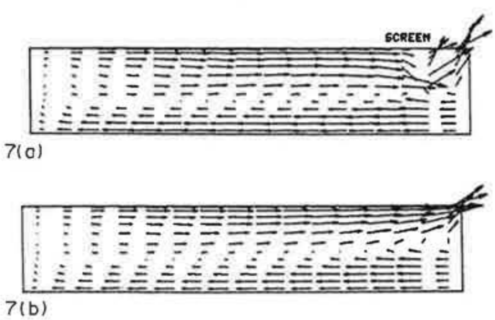

Fig. 7. Side view of velocity vectors ($x = 0.8$, normalized). (a) With screen: maximum velocity is 3.9 m/s. (b) Without screen: maximum velocity is 4.4 m/s.

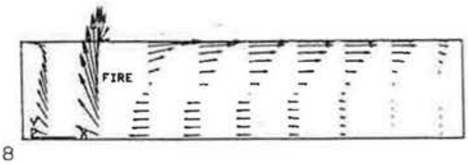

Fig. 8. Front view of velocity vectors ($z = 0.1$, normalized) no screen.

Figure 9 presents, in perspective view, plots of streamlines, and velocity vectors for the case with the screen in place. The streamline plots show the paths of fluid particles originating at particular locations. Ten equally spaced paths are shown originating at a line with normalised coordinates (0.5, 0.1, 0.99) and (0.99, 0.1, 0.99).

The presented results reveal that the general patterns predicted are physically correct and qualitatively realistic. It can be concluded, for example, that the effect of a design change such as placing a vertical screen at the mall is significant in determining the smoke spread and removal.

As a demonstration of the capability of the transient mode of operation, Fig. 10 shows the development of the 100°C rise temperature surface with time. At 20 s from ignition the 100°C surface surrounds the source and has just started to spread under the ceiling. By 30 s it has reached into the mall and is just turning the right-angled bend. At 50 s the screen has almost been reached and by 70 s the surface can clearly be seen to have come down nearer the floor and to dip down under the screen.

4.2. *Room fire*

The model was used in the steady state mode to predict conditions in Steckler's [13] room fire experiments (see plan view, Fig. 2). The compartment is 2.8 m square by 2.18 m high. On one face is situated a doorway opening 1.83 m high by either 0.74 m or 0.99 m wide in these comparisons. A steady volumetric heat source of output ranging from 31.6 kW to 158 kW was situated at the centre of the room covering a floor area of 0.09 m^2. Heat release was again varied with height according to the relationships of Cox and Chitty [14].

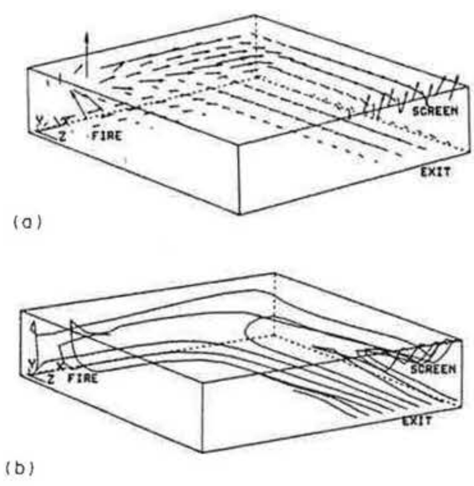

Fig. 9. Velocity vectors and streamlines for the case with the screen in place. (a) Velocity vectors at two x–z planes ($y = 0.15$ and 0.8, normalized). (b) Streamlines starting at (0.5, 0.1, 0.99) and finishing at (0.99, 0.1, 0.99).

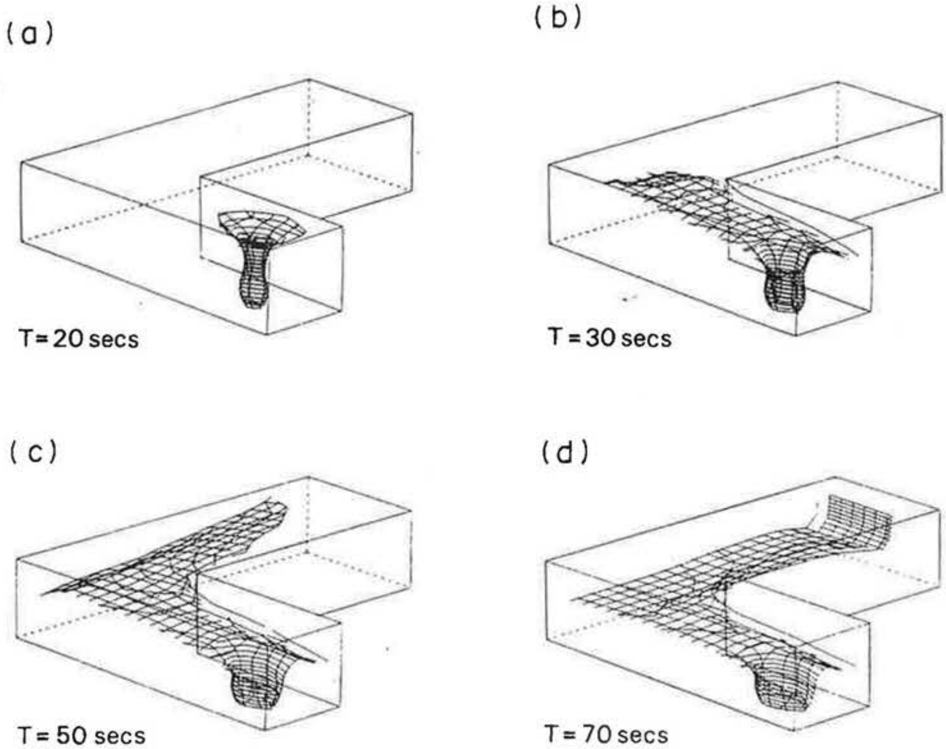

Fig. 10. Spread of smoke with time.

An adiabatic boundary condition was used at the walls since some effort had been made to minimise wall losses in the experiments. Several grid meshes were employed to test sensitivity of the solutions to grid refinement.

Figure 11 shows predicted temperature and w-velocity component on the centreline of the doorway opening for three meshes of 1872, 2340 and 6270 nodes. Although some differences do result the effects can be seen to be quite small. Typical comparisons of predictions of

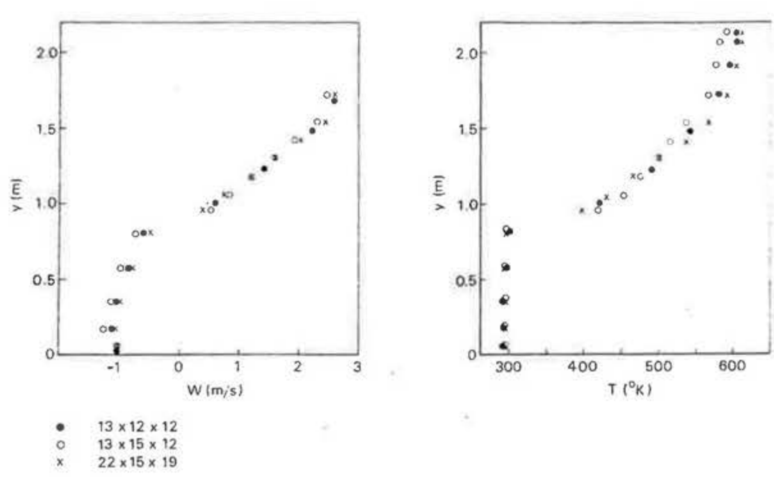

Fig. 11. Doorway centreline velocity and temperature profiles—effect of grid refinement.

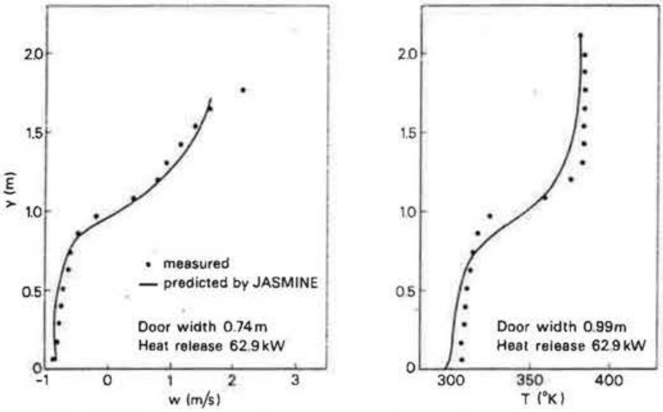

Fig. 12. Doorway velocity and corner temperature profiles.

velocity and temperature with experiments for the 63 kW fire are shown in Fig. 12 using the coarse ($13 \times 12 \times 12$) grid. The agreement can be seen to be reasonably satisfactory with small differences emerging in the velocity field just beneath the doorway soffit and also in the temperature gradient between hot and cold layers.

Of considerable interest to overall comparisons with traditional treatments and with simpler zone models is the overall mass efflux at the doorway. Figure 13 shows predictions of the present code (JASMINE) using the $13 \times 12 \times 12$ grid together with those of the Mark V version of the Harvard zone model quoted by Rockett [16], and the experimental measurements. Both models predict the correct trend with increasing heat release rate but the field model can be seen to be more accurate in this comparison.

5. CONVERGENCE AND COMPUTING REQUIREMENTS

Convergence was easily obtained for all cases, using under-relaxation on all variables. The relaxation employed was of the 'false time-step' type, which adds a 'false-transient' term into

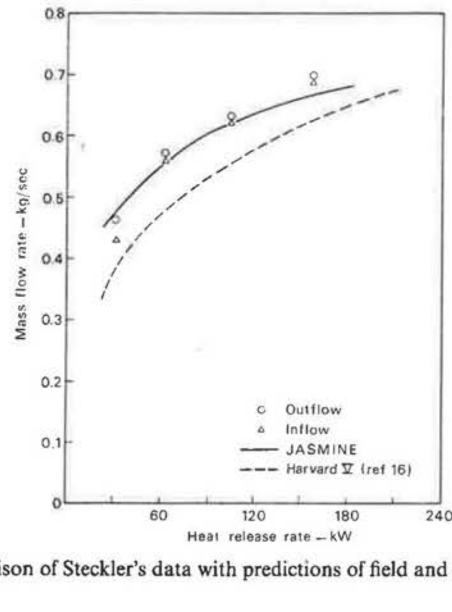

Fig. 13. Comparison of Steckler's data with predictions of field and zone models.

the finite-domain equations. The 'false time-step' used was of the order of the fluid 'residence time' in the smallest cell in the domain. Between 300 and 500 sweeps were required to obtain convergence from the initial guesses outlined above for the steady-state cases, depending on grid-size and heat output used. Approximately 10 sweeps per time step were sufficient to obtain convergence at a time step for the transient runs. A time-step of 1 s was used.

The importance of the initial guess on the number of sweeps required for convergence cannot be overemphasized. Thus, the run with the vertical screen in place, using as initial conditions the solution without the screen, required only 100 sweeps of the domain for full convergence.

The program has been run on a variety of mini-computers (Perkin–Elmer 3220, Prime 550 and Vax 11/780). The runs for the shopping mall were performed on the Perkin–Elmer machine. Run times obviously depend upon the number of cells and time steps in the problem and the number of sweeps of the domain to procure convergence. On this machine the CPU time required per cell, per sweep, per variable was approximately 4.2 ms. The program operates at different levels of dynamically-allocated storage for variables, from all in-core to fully out-of-core. The minimum core size required for the $9 \times 12 \times 16$ grid was 260 kilobytes, of which 50 kilobytes was for the storage of variables, with the remainder taken by the program object code. The out-of-core variables amounted to 166 kilobytes.

The room-fire runs were performed on the PRIME 550. On this machine the CPU time was approximately 5.3 ms/sweep/cell/variable or approximately 5 h for the $(13 \times 12 \times 12)$ grid, requiring 300 sweeps to procure convergence for the steady state.

6. CONCLUSIONS

The objective of the work was to establish the feasibility and practicability of three-dimensional field modelling of strongly buoyant, recirculating flows in realistic geometries. This objective has been accomplished, and the results of a first application of the model indicate the correct trends. Results from the two-dimensional work [2] showed reasonable agreement with two-dimensional experimental data, but data from two-dimensional experiments are scarce and insufficient to test the approach adequately. The present model will allow the rigorous validation with the wide body of three-dimensional data available from full-scale experiments. Some comparisons of grid-independent results with experiments have been presented, and appear satisfactory. Current effort is directed towards further validation. Furthermore, grid-independent results were obtained within reasonable computer resources, requiring modest storage and few hours on a minicomputer.

The choice of an implicit scheme for treating time-dependent fire phenomena is a desideratum. Since typical time scales are of the order of 1 s [17], a conflict would arise otherwise between the small time steps essential for converging explicit schemes and the longer time required to time-average the fluctuations in the flow.

Experience of the validity of the turbulence model in dealing with these strongly buoyant flows is particularly needed. Once confidence has been established in modelling these phenomena the model can then easily be extended to encompass radiation transfer and combustion modelling.

Successful validation will allow this approach to determine suitable smoke control measures on building types not specifically covered by existing regulatory codes, as for example, prison buildings, atrium hotels, etc, which require specialist advice.

Acknowledgement—This paper forms part of the work of the Fire Research Station, Building Research Establishment, Department of the Environment, UK. It is contributed by permission of the Director, Building Research Establishment.

REFERENCES

1. H. W: Emmons, The prediction of fires in buildings, in *Seventeenth Symposium (International) on Combustion*, p. 1101. The Combustion Institute, 1979.
2. N. C. Markatos, M. R. Malin and G. Cox, Mathematical modelling of buoyancy-induced smoke flow in enclosures. *Int. J. Heat Mass Transfer* **25**(1), 63–75 (1982).
3. F. H. Harlow and P. I. Nakayama, Transport of turbulence energy decay rate, LA-3854 Los Alamos Sci. Lab. University of California (1968).
4. B. E. Launder and D. B. Spalding, The numerical computation of turbulent flows. *Comp. Meths Appl. Mech. Engng* **3**, 269–289 (1974).
5. N. C. Markatos, Transient flow and heat transfer of liquid sodium coolant in the outlet plenum of a fast nuclear reactor. *Int. J. Heat Mass Transfer* **21**, 1565–1579 (1978).
6. S. V. Patankar and D. B. Spalding, A calculation procedure for heat, mass and momentum transfer in parabolic flows. *Int. J. Heat Mass Transfer* **15**, 1787–1806 (1972).
7. D. B. Spalding, Numerical computation of multiphase flow and heat transfer, in *Recent Advances in Numerical Methods in Fluids* (Edited by C. Taylor and K. Morgan) Vol. 1. Pineridge Press, London (1980).
8. D. B. Spalding, Mathematical modelling of fluid mechanics, heat transfer and mass transfer processes, Imperial College, CFDU Report HTS/80/1 (1980).
9. B. E. Launder and D. B. Spalding, *Mathematical Models of Turbulence*. Academic Press, London (1972).
10. A. S. Monin and A. M. Obukov, Basic laws of turbulent mixing in the ground layer of the atmosphere. *Trudy Geofiz. Inst. An.—SSR* **151**(24), 163–187 (1954).
11. C. L. V. Jayatillaka, The influence of Prandtl number and surface roughness on the resistance of the laminar sublayer to momentum and heat transfer, Progress in Heat and Mass Transfer (Edited by U. Grigull and E. Hahne) Vol. 1. Pergamon Press, New York (1969).
12. A. J. M. Heselden, H. G. H. Wraight and P. R. Watts, Fire problems of pedestrian precincts, Joint Fire Research Organization Fire Research Note No. 954 (1972).
13. K. D. Steckler, J. G. Quintiere and W. J. Rinkinen, Flow induced by fire in a compartment, National Bureau of Standards NBSIR 82-2520 (1982).
14. G. Cox and R. Chitty, A study of the deterministic properties of unbounded fire plumes, *Combust. Flame* **39**, 191 (1980).
15. N. C. Markatos, Computer simulation of turbulent fluid flow in chemical reactors, in *Proc. 2nd World Congress of Chem. Engng*, Vol. 5, pp. 301–312 (1981); also in *Adv. Engng Software* **5**(1), p. 32 (1983).
16. J. A. Rockett, Modelling of NBS matress tests with the Harvard Mark V fire simulation, National Bureau of Standards NBSIR 81-2440 (1981).
17. G. Cox and R. Chitty, Some stochastic properties of fire plumes. *Fire Materials* **6**, 127 (1982).